AIAA JOURNAL
Vol. 53, No. 7, July 2015

Multidimensional Flux Difference Splitting Schemes

Bernard Parent*
Pusan National University, Busan 609-735, Republic of Korea

DOI: 10.2514/1.J053584

A novel alteration to the Cauchy–Kowalevski procedure is here presented to obtain essentially monotonic solutions for multidimensional flows. It is argued that this can be accomplished by splitting the cross-derivative terms among the several dimensions, such that the coefficient of the cross derivatives remains small compared to the coefficient of the normal derivatives. The approach naturally lends itself to extending the Roe flux difference splitting scheme to multiple dimensions and is advantaged over previous Cauchy–Kowalevski-based methods by yielding a solution free of spurious oscillations in the vicinity of oblique shock waves. Several test cases ranging from low-speed subsonic flows in channels to hypersonic flows over ramp injectors indicate that the proposed genuinely multidimensional method generally achieves a twofold or more increase in resolution along each dimension over the dimensionally split Roe scheme while retaining its appealing attributes: the scheme has a compact three-node-bandwidth stencil, is a finite volume flux function, yields essentially monotonic solutions, introduces minimal dissipation within viscous layers, and is written in general matrix form. Although the method proposed is first-order accurate, it offers a resolution as high or higher than the dimensionally split second-order total-variation-diminishing schemes for many problems of interest and is expected to surpass significantly the latter when extended to second-order accuracy.

Nomenclature

A, B, C	=	flux Jacobian matrix along x, y, and z
a, b	=	wave speed along x and y
C_f	=	skin-friction coefficient
C_P	=	pressure coefficient
$\boldsymbol{F}, \boldsymbol{G}, \boldsymbol{H}$	=	flux vector along x, y, and z
f, g	=	flux along x and y
i, j, k	=	grid index along x, y, and z
L	=	left eigenvector matrix
M	=	Mach number
O	=	truncation error
P	=	pressure
p	=	order of accuracy
R	=	right eigenvector matrix
Re_x	=	Reynolds number along x
S	=	surface area of computational domain
T	=	temperature
t	=	time
$\boldsymbol{U}$	=	vector of conserved variables
u	=	conserved variable
x, y, z	=	Cartesian coordinate
α	=	parameter related to obtaining essentially monotone solutions
β	=	parameter related to the splitting of the second derivatives
γ	=	ratio of the specific heats
$\Delta x, \Delta y, \Delta z$	=	grid spacing along x, y, and z
δ	=	entropy correction factor
ϵ	=	grid-induced error
Λ	=	eigenvalue matrix
ρ	=	density

Subscripts

c	=	coarse mesh
f	=	fine mesh
∞	=	freestream conditions

Received 29 April 2014; revision received 27 August 2014; accepted for publication 15 September 2014; published online 19 December 2014.

*Dept. of Aerospace Engineering; bernparent@gmail.com.

I. Introduction

MULTIDIMENSIONAL differential equations are commonly discretized by splitting the derivatives along each dimension and discretizing the so-obtained one-dimensional derivatives using one-dimensional operators. Referred to as "dimensional splitting," such a strategy suffers from being particularly dissipative when the grid is misaligned with the waves. This entails excessive grid refinement, and hence excessive computational effort, to correctly capture flows with waves propagating oblique to the grid lines. To remedy this problem, several genuinely multidimensional alternatives (i.e., multidimensional schemes that do not resort to dimensional splitting) have thus been proposed.

One approach that has been successful at reducing the dissipation of dimensional splitting is the rotation-interpolation method. Instead of calculating the fluxes in a coordinate system that is aligned with the grid, as is done with dimensional splitting, the fluxes are determined in a coordinate system that is rotated with respect to the grid through an interpolation of the node properties [1]. This can be extended to systems of conservation laws by solving a Riemann problem at the interfaces of the rotated cell [2–4]. The rotated Riemann solver approach has some advantages over dimensional splitting. For instance, in [2], it is shown that a first-order-accurate rotated Riemann solver achieves a resolution approaching the one of a higher-order MUSCL scheme when solving expansion fans and shocks. Further, in [3], it is demonstrated that a rotated Roe scheme has an advantage over its dimensionally split analog by being free of the aphysical carbuncle phenomenon. However, because the rotational frame is the same for all variables (the frame is typically rotated following the flow velocity), the rotated Riemann solver cannot capture all waves with a high resolution. For instance, the results obtained in [4] show that substituting a dimensionally split method by a rotated Riemann solver can be a mixed blessing: although it does improve the resolution of shock waves, it results in a poorer resolution of nonaligned shear waves.

Another approach that can be used to extend the Riemann solver to multiple dimensions is "residual distribution," as first proposed by Roe [5] and later improved by Deconinck et al. [6], Abgrall and Mezine [7], and Abgrall [8]. The residual distribution scheme treats the Riemann problem at the cell's interface in a genuinely multidimensional manner. This is accomplished by distributing the flux integral at the cells interfaces (the residual) to the neighboring nodes in a downwind manner, with the direction of downwinding being function of the waves within the Riemann solver. This yields advantages over dimensionally split methods: much less dissipation is introduced both at low and high Mach numbers (see, for instance, [9,10]), and the stencil is more compact for the same level of

resolution. But, there are also disadvantages associated with residual distribution, such as more frequent convergence hangs in obtaining a steady-state solution [11] and the difficulty of incorporating viscous effects. Including the viscous terms poses some problems due to the elliptic nature of the diffusion derivatives not being compatible with the hyperbolic nature of residual distribution, although some progress is being made in this area. For instance, one approach is presented in [12], where the diffusion terms are added through a Petrov–Galerkin scheme; and a second strategy is proposed in [13–15], where the viscous terms are expressed as a first-order hyperbolic system instead of a second-order diffusion system, making their inclusion within a residual distribution scheme straightforward. Thus, the residual distribution schemes can be seen to depart significantly from finite volume schemes to resemble more finite element methods. Substituting the dimensionally split finite volume flux functions by a residual distribution strategy in the current computational fluid dynamics codes is hence not a trivial matter: not only would this require a substantial change in the architecture of the code, but it is not clear how (if at all) the convergence acceleration techniques currently used can be extended to residual distribution methods. Perhaps for these reasons, the adoption of residual distribution has been somewhat limited thus far.

Yet another class of multidimensional schemes has been developed, albeit from a different standpoint. In contrast to the rotation-interpolation and residual distribution methods, it does not make use of the Riemann solver and its associated wave speeds, but rather it consists of the application of the Cauchy–Kowalevski procedure to multidimensional equations as first proposed by Lax and Wendroff [16]. This was subsequently improved by Richtmyer [17] through a combination with a predictor–corrector method (the so-called Lax–Wendroff predictor–corrector method), which was further enhanced by Smolarkiewicz [18], Colella [19], and Leveque [20]. Among the latter, the multidimensional positive definite advection transport algorithm schemes by Smolarkiewicz [18] continue to be used in simulating geophysical flows [21,22] and have been extended recently to other types of physical models, including compressible flows [23]. Such methods can be considered to be a form of predictor–corrector, with the predictor step being a first-order-accurate donor-cell approximation and the following corrector steps estimating and compensating the truncation error introduced by the previous steps in order to obtain higher-order accuracy. Because the estimation and correction of the truncation error within the second and subsequent steps are performed on the stencil as a whole (including all temporal and spatial derivatives), the method is a genuinely multidimensional predictor–corrector method. Although such a strategy has had some success in simulating several flowfields, it does suffer, like its one-dimensional analog, from several drawbacks compared to flux difference splitting schemes and other Riemann solvers. Namely, it is not monotonicity preserving for systems of conservation laws, and because of its predictor–corrector formulation effectively making the fluxes at the interface function of the Courant–Friedrichs–Lewy (CFL) number, it is not compatible with the commonly used convergence acceleration techniques such as block-implicit approximate factorization, Jacobian-free–Newton–Krylov, lower–upper symmetric Gauss–Seidel (LUSGS), multigrid, etc. Another method based on the Cauchy–Kowalevski procedure that can be regrouped with the latter is the scheme by Ni [24] that, despite not being a predictor–corrector method, does suffer like the aforementioned schemes from the fluxes at the interface being a function of the CFL number.

To overcome the limitations of the latter schemes derived from the Cauchy–Kowalevski procedure, a technique is presented in [25] in which the time step that naturally appears within the flux function is replaced by a characteristic time step. The characteristic time step is specified in such a way that the converged solution does not depend on the CFL number. In doing so, the Lax–Wendroff method can be used in conjunction with the convergence acceleration techniques devised for finite volume schemes. However, the use of the characteristic time step in [25] is observed to lead to stability issues and to require the addition of arbitrary scalar artificial dissipation terms to prevent even–odd node discoupling. This is avoided in [26], where Huang and Lerat derived a characteristic time step such that the flux obtained with the Cauchy–Kowalevski technique collapses to the Roe scheme for one-dimensional (1-D) systems. In this manner, there is no need to add extra dissipation terms to prevent even–odd node discoupling of the properties, and the method can capture contact surfaces with as high a resolution as the Roe scheme. Nonetheless, the method by Huang and Lerat is not monotonic, with the consequence that it leads to significant undershoots and overshoots of the properties near shock waves when the latter are not aligned with the grid lines.

Although the multidimensional approaches outlined previously are promising and may lead to capable methods in the future, neither one has been widely deployed, albeit for different reasons: the rotated Riemann solver is not truly multidimensional and cannot capture all waves with high resolution, the residual distribution strategy resembles a finite element scheme and requires significant changes to the architecture of the existing finite volume codes, and the multidimensional extension of the predictor–corrector Lax–Wendroff scheme is not compatible with the acceleration techniques generally used for compressible flows, whereas the corrected Cauchy–Kowalevski procedure using a characteristic time step results in a nonmonotone solution near oblique shock waves.

As a means to address these shortcomings, a novel genuinely multidimensional finite-volume method is here proposed. The method proposed consists of altering the Cauchy–Kowalevski procedure in order to obtain monotonicity for multidimensional flows without resorting to the use of limiter functions. It is here argued that this can be accomplished by splitting the cross-derivative terms among the several dimensions such that the coefficient of the cross derivatives remains small compared to the coefficient of the normal derivatives. The approach is then seen to naturally lend itself to extending the Roe flux difference splitting scheme to multiple dimensions. Several test cases of subsonic, supersonic, and hypersonic inviscid and viscous flows are then presented to assess the increase in resolution of the proposed multidimensional Roe scheme over its dimensionally split counterpart.

II. Derivation of the Discretization Equation

Using the Cauchy–Kowalevski procedure ([27] sec. 19.3), it is here desired to determine an adequate discretization equation for a hyperbolic conservation law in two dimensions, as first obtained by Lax and Wendroff in [16]. For this purpose, consider a scalar conservation law solving the variable u:

$$\frac{\partial u}{\partial t} + a\frac{\partial u}{\partial x} + b\frac{\partial u}{\partial y} = 0 \tag{1}$$

where a and b are the wave speeds along the Cartesian coordinates x and y, respectively. For simplicity, let us consider the case of constant wave speeds, and let us first discretize the temporal derivative using a first-order forward operator and the spatial derivatives using centered stencils as follows:

$$\frac{u^{n+1} - u^n}{\Delta t} + a\frac{u_{i+1} - u_{i-1}}{2\Delta x} + b\frac{u_{j+1} - u_{j-1}}{2\Delta y} = 0 \tag{2}$$

In the latter, the node indices i, j, and n are implied. For instance, the notation u_{i+1} refers to the property u at the node $(i+1, j)$ at the time level n, whereas the notation u^{n+1} refers to the property u at the node (i, j) at the time level $n+1$. Each discretization stencil within Eq. (2) can be expanded using Taylor series:

$$\frac{u^{n+1} - u^n}{\Delta t} = \frac{\partial u}{\partial t} + \frac{\Delta t}{2}\frac{\partial^2 u}{\partial t^2} + O(\Delta t^2) \tag{3}$$

$$\frac{u_{i+1} - u_{i-1}}{2\Delta x} = \frac{\partial u}{\partial x} + O(\Delta x^2) \tag{4}$$

$$\frac{u_{j+1}-u_{j-1}}{2\Delta y}=\frac{\partial u}{\partial y}+O(\Delta y^2) \tag{5}$$

After substituting the latter in the discretization equation [Eq. (2)], the following is obtained:

$$\frac{\partial u}{\partial t}+a\frac{\partial u}{\partial x}+b\frac{\partial u}{\partial y}=-\frac{\Delta t}{2}\frac{\partial^2 u}{\partial t^2}+O(\Delta t^2,\Delta x^2,\Delta y^2) \tag{6}$$

Now, seek to rewrite the term involving the second derivative in time as a spatial derivative. For this purpose, take the derivative of Eq. (6) with respect to t, x, and y:

$$\frac{\partial^2 u}{\partial t^2}+a\frac{\partial^2 u}{\partial t\partial x}+b\frac{\partial^2 u}{\partial t\partial y}=O(\Delta t,\Delta x,\Delta y) \tag{7}$$

$$\frac{\partial^2 u}{\partial t\partial x}+a\frac{\partial^2 u}{\partial x^2}+b\frac{\partial^2 u}{\partial x\partial y}=O(\Delta t,\Delta x,\Delta y) \tag{8}$$

$$\frac{\partial^2 u}{\partial t\partial y}+a\frac{\partial^2 u}{\partial x\partial y}+b\frac{\partial^2 u}{\partial y^2}=O(\Delta t,\Delta x,\Delta y) \tag{9}$$

In the latter, the higher-order terms are discarded because they will subsequently not be needed. Multiply Eqs. (8) and (9) by $-a$ and $-b$, respectively. Then, add the resulting equations to Eq. (7), isolate $\partial^2 u/\partial t^2$ and simplify

$$\frac{\partial^2 u}{\partial t^2}=a^2\frac{\partial^2 u}{\partial x^2}+b^2\frac{\partial^2 u}{\partial y^2}+2ab\frac{\partial^2 u}{\partial x\partial y}+O(\Delta t,\Delta x,\Delta y) \tag{10}$$

Substitute the latter in Eq. (6) to obtain the modified equation

$$\begin{aligned}&\frac{\partial u}{\partial t}+a\frac{\partial u}{\partial x}+b\frac{\partial u}{\partial y}\\&=-\frac{\Delta t}{2}\left(a^2\frac{\partial^2 u}{\partial x^2}+b^2\frac{\partial^2 u}{\partial y^2}+2ab\frac{\partial^2 u}{\partial x\partial y}\right)\\&\quad+O(\Delta t^2,\Delta x^2,\Delta y^2)\end{aligned} \tag{11}$$

A comparison of the latter with the original differential equation [Eq. (1)] clearly shows that the use of centered differences for the convection derivatives combined with a forward stencil for the time derivative is not second-order accurate because of the appearance of the second-derivative and cross-derivative terms within the modified equation.

Let us now make modifications to the discretization equation [Eq. (2)] in order to obtain a modified equation that collapses to the original differential equation within a second-order truncation error. We wish to do so while keeping the discretization of the temporal derivative as a first-order forward stencil, because any other type of operator for the time derivative would necessarily entail either a loss of conservation, a loss of monotonicity, or increased storage due to the dependence of the stencil on "future" values of u. In light of the appearance of second-derivative and cross-derivative terms in the modified equation obtained above, we add some second-derivative and cross-derivative stencils of the opposite sign to the discretization equation as follows:

$$\begin{aligned}&\frac{u^{n+1}-u^n}{\Delta t}+a\frac{u_{i+1}-u_{i-1}}{2\Delta x}+b\frac{u_{j+1}-u_{j-1}}{2\Delta y}\\&-\frac{a^2\Delta t}{2}\frac{u_{i+1}-2u_i+u_{i-1}}{\Delta x^2}\\&-\frac{b^2\Delta t}{2}\frac{u_{j+1}-2u_j+u_{j-1}}{\Delta y^2}\\&-ab\Delta t\frac{u_{i+1,j+1}-u_{i-1,j+1}-u_{i+1,j-1}+u_{i-1,j-1}}{4\Delta x\Delta y}=0\end{aligned} \tag{12}$$

Following the same steps as shown previously, it can be easily shown that the modified equation associated with the latter collapses to the original differential equation [Eq. (1)] as long as $a/\Delta x$ and $b/\Delta y$ are within the same order of magnitude.

It is emphasized that Eq. (12) is a second-order-accurate discretization of a hyperbolic equation with constant wave speeds. When applied to a hyperbolic system where the wave speeds are not constant (such as the Euler equations for instance), the second-order accuracy is not guaranteed. Nonetheless, this is not a source of concern, as the goal here is not to obtain a second-order-accurate scheme (as in [28], for instance) but rather a first-order-accurate genuinely multidimensional extension of the Roe scheme with minimal truncation error. How this can be obtained from Eq. (12) is outlined next.

III. Derivation of Flux Functions from the Discretization Equation

Because we are seeking a conservative method written in finite volume form, we wish to express the discretization equation as a difference between the fluxes at the cell's interfaces, as follows:

$$\frac{u^{n+1}-u^n}{\Delta t}+\frac{f_{i+1/2}-f_{i-1/2}}{\Delta x}+\frac{g_{j+1/2}-g_{j-1/2}}{\Delta y}=0 \tag{13}$$

where f and g are the fluxes along x and y, respectively. To do so, first rewrite the discretization equation [Eq. (12)] in the following form:

$$\begin{aligned}&\frac{u^{n+1}-u^n}{\Delta t}+a\frac{u_{i+1}+u_i}{2\Delta x}-a\frac{u_i+u_{i-1}}{2\Delta x}+b\frac{u_{j+1}+u_j}{2\Delta y}\\&-b\frac{u_j+u_{j-1}}{2\Delta y}-a^2\frac{\Delta t}{\Delta x}\frac{u_{i+1}-u_i}{2\Delta x}+a^2\frac{\Delta t}{\Delta x}\frac{u_i-u_{i-1}}{2\Delta x}\\&-b^2\frac{\Delta t}{\Delta y}\frac{u_{j+1}-u_j}{2\Delta y}+b^2\frac{\Delta t}{\Delta y}\frac{u_j-u_{j-1}}{2\Delta y}\\&-\beta_{xy}ab\Delta t\frac{u_{i+1,j+1}+u_{i-1,j-1}-u_{i-1,j+1}-u_{i+1,j-1}}{4\Delta x\Delta y}\\&-(1-\beta_{xy})ab\Delta t\frac{u_{i+1,j+1}+u_{i-1,j-1}-u_{i-1,j+1}-u_{i+1,j-1}}{4\Delta x\Delta y}=0\end{aligned} \tag{14}$$

where β_{xy} is a parameter related to the splitting of the cross-derivative terms among the several dimensions in order to obtain monotonicity. The value that needs to be given to β_{xy} to achieve monotonicity will be outlined in a later section. Note that, independent of the value given to β_{xy}, the latter equation will yield exactly the same solution as Eq. (12). Now, we can split the cross-derivative terms function of β_{xy} as follows:

$$\begin{aligned}&-\beta_{xy}ab\Delta t\frac{u_{i+1,j+1}+u_{i-1,j-1}-u_{i-1,j+1}-u_{i+1,j-1}}{4\Delta x\Delta y}\\&=-\beta_{xy}ab\frac{\Delta t}{\Delta y}\frac{u_{i+1,j+1}-u_{i+1,j-1}+u_{i,j+1}-u_{i,j-1}}{4\Delta x}\\&\quad+\beta_{xy}ab\frac{\Delta t}{\Delta y}\frac{u_{i,j+1}-u_{i,j-1}+u_{i-1,j+1}-u_{i-1,j-1}}{4\Delta x}\end{aligned} \tag{15}$$

$$-(1-\beta_{xy})ab\Delta t\frac{u_{i+1,j+1}+u_{i-1,j-1}-u_{i-1,j+1}-u_{i+1,j-1}}{4\Delta x\Delta y}$$
$$=-(1-\beta_{xy})ab\frac{\Delta t}{\Delta x}\frac{u_{i+1,j+1}-u_{i-1,j+1}+u_{i+1,j}-u_{i-1,j}}{4\Delta y}$$
$$+(1-\beta_{xy})ab\frac{\Delta t}{\Delta x}\frac{u_{i+1,j}-u_{i-1,j}+u_{i+1,j-1}-u_{i-1,j-1}}{4\Delta y} \quad (16)$$

After substituting in Eq. (14), and comparing the resulting equation to Eq. (13), it follows that the flux functions at the interfaces correspond to

$$f_{i+1/2}=a\frac{u_{i+1}+u_i}{2}-a^2\frac{\Delta t}{\Delta x}\frac{u_{i+1}-u_i}{2}$$
$$-\beta_{xy}ab\frac{\Delta t}{\Delta y}\frac{u_{i+1,j+1}-u_{i+1,j-1}+u_{i,j+1}-u_{i,j-1}}{4} \quad (17)$$

$$g_{j+1/2}=b\frac{u_{j+1}+u_j}{2}-b^2\frac{\Delta t}{\Delta y}\frac{u_{j+1}-u_j}{2}$$
$$-(1-\beta_{xy})ab\frac{\Delta t}{\Delta x}\frac{u_{i+1,j+1}-u_{i-1,j+1}+u_{i+1,j}-u_{i-1,j}}{4} \quad (18)$$

Thus far, the discretization equation has not been modified. Indeed, should the fluxes outlined in Eqs. (17) and (18) be substituted in Eq. (13), one would obtain precisely the discretization equation outlined in Eq. (12).

IV. Alterations to the Flux Functions to Obtain Monotonicity

The fluxes derived in the previous section as outlined in Eqs. (17) and (18) suffer from not being monotonic. This becomes clear for a problem where the cross-derivative terms disappear (such as when the properties vary only along one spatial dimension). Then, choosing a very small value for the time step Δt would yield a centered finite difference stencil. This is well known to result in even–odd node discoupling of the properties, and therefore in a solution tainted with spurious oscillations. One way that this can be avoided is by ensuring that the time step at the interface is such that the resulting discretization equation obeys the rule of the positive coefficients [29]. For the flux outlined in Eq. (17) to conform to the rule of the positive coefficients, the coefficient multiplying the u_{i+1} term must be less than or equal to zero, whereas the coefficient multiplying the u_i term must be greater than or equal to zero:

$$\frac{a}{2}-\frac{a^2}{2\Delta x}\Delta t_{i+1/2}\le 0 \quad \text{and} \quad \frac{a}{2}+\frac{a^2}{2\Delta x}\Delta t_{i+1/2}\ge 0 \quad (19)$$

After isolating the time step in the latter two conditions, we obtain

$$\Delta t_{i+1/2}\ge\frac{\Delta x}{a} \quad \text{and} \quad \Delta t_{i+1/2}\ge-\frac{\Delta x}{a} \quad (20)$$

If a is negative, then the latter will prevail over the former. If a is positive, then the former will prevail over the latter. We can hence combine the latter two conditions into a single one:

$$\Delta t_{i+1/2}\ge\frac{\Delta x}{|a|} \quad (21)$$

The amount of dissipation is the least when the magnitude of the second-derivative terms is the smallest, which would occur when the time step is the smallest. Therefore, the least dissipative method would be obtained when the time step is set as follows:

$$\Delta t_{i+1/2}=\frac{\Delta x}{|a|} \quad (22)$$

Following similar steps, it can be shown that the optimal time step at the $j+1/2$ interface corresponds to

$$\Delta t_{j+1/2}=\frac{\Delta y}{|b|} \quad (23)$$

It is noted that the latter two equations essentially define the grid spacings Δx and Δy for a given time step $\Delta t=\Delta t_{i+1/2}=\Delta t_{j+1/2}$. Should the grid spacing be specified differently, the resulting discretization equation would still yield a solution that is monotonic, but the truncation error would be more significant.

After substituting $\Delta t_{i+1/2}$ and $\Delta t_{j+1/2}$ in Eqs. (17) and (18), respectively, the fluxes become

$$f_{i+1/2}=a\frac{u_{i+1}+u_i}{2}-|a|\frac{u_{i+1}-u_i}{2}$$
$$-\beta_{xy}\frac{ab}{|a|}\frac{\Delta x}{\Delta y}\frac{u_{i+1,j+1}-u_{i+1,j-1}+u_{i,j+1}-u_{i,j-1}}{4} \quad (24)$$

$$g_{j+1/2}=b\frac{u_{j+1}+u_j}{2}-|b|\frac{u_{j+1}-u_j}{2}$$
$$-(1-\beta_{xy})\frac{ab}{|b|}\frac{\Delta y}{\Delta x}\frac{u_{i+1,j+1}-u_{i-1,j+1}+u_{i+1,j}-u_{i-1,j}}{4} \quad (25)$$

In the fluxes outlined in Eqs. (24) and (25), the first-derivative and the second-derivative terms (the first two terms on the right-hand side) respect the rule of the positive coefficients and lead to a monotonic flux function. However, the cross-derivative terms (all the term functions of β) do not obey the rule of the positive coefficients. Further, it can be demonstrated that no value given to β would yield a discretization equation with all-positive coefficients. One way that the method could be made monotonicity preserving is by limiting the cross-derivative terms such that the resulting fluxes obey the total-variation-diminishing (TVD) condition. Numerical experiments indicate, however, that such a strategy results in erratic limiter behavior often prevents a converged solution. An alternative novel method is here proposed that yields essentially monotone solutions while not being subject to convergence hangs. The method consists of defining β such that the magnitude of the cross-derivative coefficient is not superior to the magnitude of the second-derivative coefficient. This results in solutions that are essentially monotonic because the spurious oscillations that may originate from the cross-derivative terms are damped by the dissipation introduced by the second-order terms.

For the flux function outlined in Eq. (24), the cross-derivative coefficient can be compared to the second-derivative coefficient through the following condition:

$$\alpha\left|\beta_{xy}\frac{ab}{4|a|}\frac{\Delta x}{\Delta y}\right|\le\frac{|a|}{2} \quad (26)$$

where α is an arbitrary parameter multiplying the cross-derivative coefficient. The latter should be understood as a condition on α given a certain β_{xy}: the higher α is allowed to be, the lower the cross-derivative coefficient will be when compared to the second-derivative coefficient. For the case of β_{xy} positive, it can be easily shown that condition (26) can be rewritten to

$$\alpha\le\frac{1}{\beta_{xy}}\frac{2|a|\Delta y}{|b|\Delta x} \quad (27)$$

This corresponds to the first condition on the parameter α. The second condition can be obtained starting from the flux function outlined in Eq. (25), in which a comparison between the cross-derivative coefficient to the second-derivative coefficient yields the following condition:

$$\alpha\left|(1-\beta_{xy})\frac{ab}{4|b|}\frac{\Delta y}{\Delta x}\right|\le\frac{|b|}{2} \quad (28)$$

Then, for $(1-\beta_{xy})$ positive, a second condition on α can be obtained:

$$\alpha \leq \frac{1}{1-\beta_{xy}} \frac{2|b|\Delta x}{|a|\Delta y} \tag{29}$$

Now, we wish to find a formulation for β_{xy} that would permit the lowest possible value for α in conditions (27) and (29). Consider the following definition of β_{xy}:

$$\beta_{xy} \equiv \frac{|a|\Delta y}{|a|\Delta y + |b|\Delta x} \tag{30}$$

which is such that the aforementioned constraints $\beta_{xy} \geq 0$ and $(1 - \beta_{xy}) \geq 0$ are satisfied. Then, after substituting the latter in conditions (27) and (29), we get

$$\alpha \leq \frac{2(|a|\Delta y + |b|\Delta x)}{|b|\Delta x} \quad \text{and} \quad \alpha \leq \frac{2(|a|\Delta y + |b|\Delta x)}{|a|\Delta y} \tag{31}$$

The most stringent condition on α would occur when a is zero for the first condition and when b is zero for the second condition. When this occurs, both conditions would yield the following:

$$\alpha \leq 2 \tag{32}$$

Therefore, by specifying β_{xy} as in Eq. (30), α can be set to a value as high as two and conditions (26) and (28) will be satisfied. Recalling that α is an arbitrary coefficient multiplying the cross-derivative terms (in doing a comparison with the second-derivative terms), it follows that the magnitude of the coefficient multiplying the cross-derivative terms will be, at most, half the magnitude of the coefficient multiplying the second-derivative terms should β_{xy} be specified as in Eq. (30). Therefore, by specifying β_{xy} as was done herein, it is unlikely that the magnitude of the cross-derivative terms significantly exceeds the one of the second-derivative terms.

Then, substitute β_{xy} in the fluxes outlined in Eqs. (24) and (25), and simplify

$$f_{i+1/2} = a\frac{u_{i+1} + u_i}{2} - |a|\frac{u_{i+1} - u_i}{2} - \frac{ab\Delta x}{|a|\Delta y + |b|\Delta x}\frac{u_{i+1,j+1} - u_{i+1,j-1} + u_{i,j+1} - u_{i,j-1}}{4} \tag{33}$$

$$g_{j+1/2} = b\frac{u_{j+1} + u_j}{2} - |b|\frac{u_{j+1} - u_j}{2} - \frac{ab\Delta y}{|a|\Delta y + |b|\Delta x}\frac{u_{i+1,j+1} - u_{i-1,j+1} + u_{i+1,j} - u_{i-1,j}}{4} \tag{34}$$

Although not monotonicity preserving in the strict sense following Harten's definition, numerical experiments indicate that the latter flux functions yield a solution that is essentially free of spurious oscillations. Several comparisons were performed between the proposed method and the dimensional-splitting strategy when solving a scalar conservation law, not only for a constant-coefficient test case but also for several other test cases in which the coefficients were not constant and given an arbitrary spatial distribution including discontinuities. It is found that the proposed method yields a resolution being significantly superior to the one obtained with dimensionally split first-order upwinded stencils. In fact, despite being first-order accurate, the present approach is found to yield a resolution that is essentially the same as the one of dimensionally split second-order TVD stencils whenever the waves propagate obliquely to the grid lines. Although the cross-derivative terms may introduce small aphysical oscillations near sharp gradients, such oscillations are barely discernible and are quickly damped by the second-derivative terms.

V. Proposed Multidimensional Flux Difference Splitting Schemes

The fluxes derived in the previous section for a scalar conservation law are now extended to a system of conservation laws of the form:

$$\frac{\partial \boldsymbol{U}}{\partial t} + \frac{\partial \boldsymbol{F}}{\partial x} + \frac{\partial \boldsymbol{G}}{\partial y} = 0 \tag{35}$$

where $\boldsymbol{U}$ is the vector of conserved variables, whereas $\boldsymbol{F}$ and $\boldsymbol{G}$ are the convective flux vectors along x and y, respectively. When written in finite volume form, the discretization equation associated with the latter becomes

$$\frac{\boldsymbol{U}^{n+1} - \boldsymbol{U}^n}{\Delta t} + \frac{\boldsymbol{F}_{i+1/2} - \boldsymbol{F}_{i-1/2}}{\Delta x} + \frac{\boldsymbol{G}_{j+1/2} - \boldsymbol{G}_{j-1/2}}{\Delta y} = 0 \tag{36}$$

where $\boldsymbol{F}_{i+1/2}$ and $\boldsymbol{G}_{j+1/2}$ denote the flux functions at the interfaces perpendicular to the x and y axes, respectively. In the latter, the time derivative can be seen to be discretized using a first-order forward stencil. This is not an arbitrary choice. Because the Cauchy–Kowalevski procedure aims to discretize a sum of partial derivatives including the time derivative rather than the spatial derivatives independently of the time derivative, and because the proposed scheme was derived by fixing the time derivative to first-order forward [as specified in Sec. II, just before Eq. (12)], it would not be adequate to use another type of stencil than first-order forward for the time derivative.

It is desired that the flux functions satisfy the following two conditions:

1) They should collapse to the Roe scheme [30] when there are no gradients in the second dimension.

2) They should collapse to the fluxes derived previously in Eqs. (33) and (34) when solving a single scalar conservation law with constant coefficients.

One approach that satisfies the latter two conditions is the following:

$$\boldsymbol{F}_{i+1/2} = \frac{1}{2}(\boldsymbol{F}_i + \boldsymbol{F}_{i+1}) - \frac{1}{2}|A|_{i+1/2}(\boldsymbol{U}_{i+1} - \boldsymbol{U}_i) - \frac{1}{4}B_{i+1/2}\left(\frac{\Delta y}{\Delta x}|A|_{i+1/2} + |B|_{i+1/2}\right)^{-1} A_{i+1/2}(\boldsymbol{U}_{i+1,j+1} - \boldsymbol{U}_{i+1,j-1} + \boldsymbol{U}_{i,j+1} - \boldsymbol{U}_{i,j-1}) \tag{37}$$

$$\boldsymbol{G}_{j+1/2} = \frac{1}{2}(\boldsymbol{G}_j + \boldsymbol{G}_{j+1}) - \frac{1}{2}|B|_{j+1/2}(\boldsymbol{U}_{j+1} - \boldsymbol{U}_j) - \frac{1}{4}A_{j+1/2}\left(\frac{\Delta x}{\Delta y}|B|_{j+1/2} + |A|_{j+1/2}\right)^{-1} B_{j+1/2}(\boldsymbol{U}_{i+1,j+1} - \boldsymbol{U}_{i-1,j+1} + \boldsymbol{U}_{i+1,j} - \boldsymbol{U}_{i-1,j}) \tag{38}$$

In the latter, A corresponds to the flux Jacobian along x:

$$A = \frac{\partial \boldsymbol{F}}{\partial \boldsymbol{U}} \tag{39}$$

and the matrix $|A|$ corresponds to the Roe matrix along x:

$$|A| = R(A)|\Lambda(A)|L(A) \tag{40}$$

where the matrices $R(A)$, $\Lambda(A)$, and $L(A)$ correspond to the right eigenvector matrix, the eigenvalue matrix, and the left eigenvector matrix of the flux Jacobian A, respectively. Similarly, the other Roe matrix $|B|$ is obtained from the flux Jacobian along y. In determining the Roe matrices at the interface, the properties are determined following the "Roe average" strategy, as specified in [30]. This improves, albeit slightly, the resolution within boundary layers compared to an arithmetic average. It may be argued that the Roe averaging technique is only applicable to 1-D flows because it is

derived for the 1-D Euler equations, and its use in a multidimensional scheme is questionable. However, Roe averaging is here useful because it permits a discontinuity to be captured without dissipation within one cell as long as the flow is aligned with the gridlines. This is particularly beneficial when simulating boundary layers near surfaces because the flow in such regions is necessarily aligned with the gridlines and because the accuracy of the solution depends significantly on the dissipation of the flux discretization. In other regions, the type of averaging (either Roe or arithmetic) is found not to cause any discernible change in the solution.

Additionally, to prevent aphysical phenomena from forming, the eigenvalues within the Roe matrices are altered using the following entropy correction:

$$|[\Lambda]_{r,r}| \rightarrow \sqrt{[\Lambda]_{r,r}^2 + \delta a^2} \tag{41}$$

where a is the speed of sound, and δ is a user-specified parameter. To prevent excessive dissipation within viscous layers, the entropy correction is applied only to the acoustic waves for the Roe matrices on the numerator of the flux functions. On the other hand, the entropy correction is applied to all waves for the Roe matrices on the denominator of the flux function (the Roe matrices part of the cross-derivative terms). It is necessary to do so (that is, to apply the entropy correction to all waves for the Roe matrices part of the cross-derivative terms) to prevent the possible formation of a singular matrix that cannot be inverted.

Substituting the fluxes outlined in Eqs. (37) and (38) in the discretization equation leads to a first-order-accurate discretization scheme with a three-node-bandwidth stencil. Because the present approach collapses to the Roe solver for 1-D systems of equations, it is first-order accurate when solving 1-D flows or multidimensional flows where the waves are aligned with the grid lines. Further, as will be demonstrated in the next section, the present method remains first-order accurate when solving flows in multiple dimensions when the waves are misaligned with the grid lines, despite yielding a resolution as high, or higher, as dimensionally split second-order TVD schemes. It is noted that a "first-order-accurate scheme" here does not necessarily denote a scheme with specific properties (such as being monotonic, linear, etc). Rather, a first-order-accurate scheme is here meant, in the more general sense, as a scheme that yields a numerical solution for which the order of accuracy does not exceed significantly one for any flowfield, with the order of accuracy determined from the rate of convergence of the numerical solution to the exact solution.

VI. Test Cases

Several test cases are now considered to assess the gain in resolution of the proposed genuinely multidimensional method over the dimensionally split Roe solver [30] and the dimensionally split Yee–Roe TVD scheme [31]. All cases presented herein consist of the steady-state solution of either the Euler equations or Navier–Stokes equations on a structured mesh using generalized curvilinear coordinates and a perfect gas model with the specific heat ratio set to 1.4 and the gas constant set to 286 J/kg · K. Additional numerical experiments indicate that the gains in resolution obtained with the proposed method over the dimensionally split approach remain unaffected when solving the flow in a time-accurate fashion.

Although the flux functions presented in Eqs. (37) and (38) are in Cartesian coordinates, they can be extended to generalized curvilinear coordinates simply by setting $\Delta x = \Delta y = 1$ and substituting the Cartesian eigenvector and eigenvalue matrices by their curvilinear analogs. Unless otherwise specified, the entropy correction factor δ is fixed to 0.3 for the acoustic waves, to zero for the nonacoustic waves, and to 0.02 for all wave parts of the matrices on the denominator of the flux function. Because the flux functions depend on the eigenvectors and eigenvalues of the convective flux Jacobian, and because the eigenvectors are not unique, it is important to use the same eigenvectors as used herein (which can be found in the appendix of [32]) in order to reproduce the results shown next. To reduce the computational effort, the results are obtained through the use of a block-implicit approximate-factorization algorithm combined with local pseudotime stepping and the marching-window acceleration technique [33]. In all cases, the convergence rate of the proposed multidimensional scheme is observed to be more or less the same as the one of the dimensional-splitting approach: no convergence hangs occur, and the CFL number can be set to essentially the same value for both methods.

A. Shear Wave

The first test case consists of a shear wave between two streams, with both streams having a pressure of 0.1 bar and a temperature of 300 K, but with one stream injected at Mach 3 and the other at Mach 2. A shear wave can be captured with minimal dissipation within one cell by the dimensionally split Roe scheme when the mesh is aligned with the velocity vector. However, when there is a misalignment between the mesh and the velocity vector, the dimensionally split approach introduces excessive dissipation. The problem is here setup such that the 60×60 mesh is at a 45 deg angle with the incoming flow vector in order to determine the amount of dissipation when the misalignment between the mesh and the velocity vector is the most significant. Since the viscosity and thermal conductivity are set to zero, the exact solution is trivial (i.e., the inflow conditions are propagated downstream unaltered, separated by a contact discontinuity). As can be seen in Fig. 1, the dimensionally split Roe and TVD methods depart significantly from the exact solution by spreading the contact discontinuity over 15 cells and 8 cells, respectively. On the other hand, the use of the proposed genuinely multidimensional method results in much closer agreement with the exact solution, with the contact surface being spread over two times fewer cells than second-order TVD schemes and four times fewer cells than the first-order Roe scheme.

B. Supersonic Flow over a Sine Wall

The improvement in resolution obtained with the proposed method is not limited to contact surfaces and shear waves, but it is apparent through shock waves and expansion fans. For instance, consider air entering a channel at a Mach number of two, a pressure of 10,200 Pa, and a temperature of 300 K. When the flow interacts with the wavy

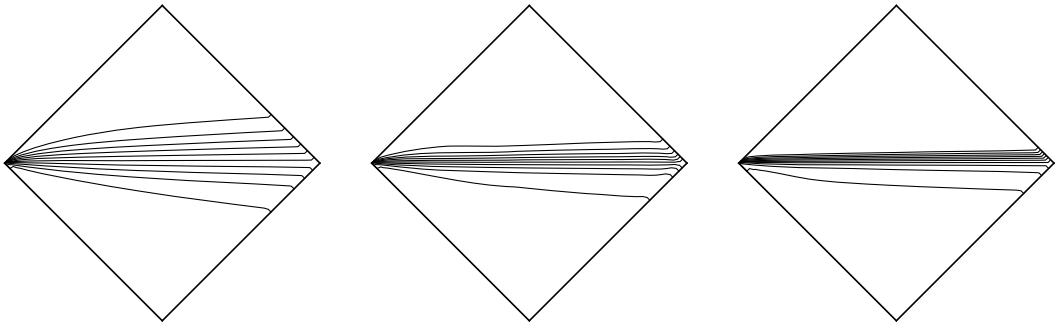

a) First-order Roe **b) Second-order TVD** **c) Proposed first-order method**

Fig. 1 Mach number contours for the shear-wave case with $\Delta M = 0.1$.

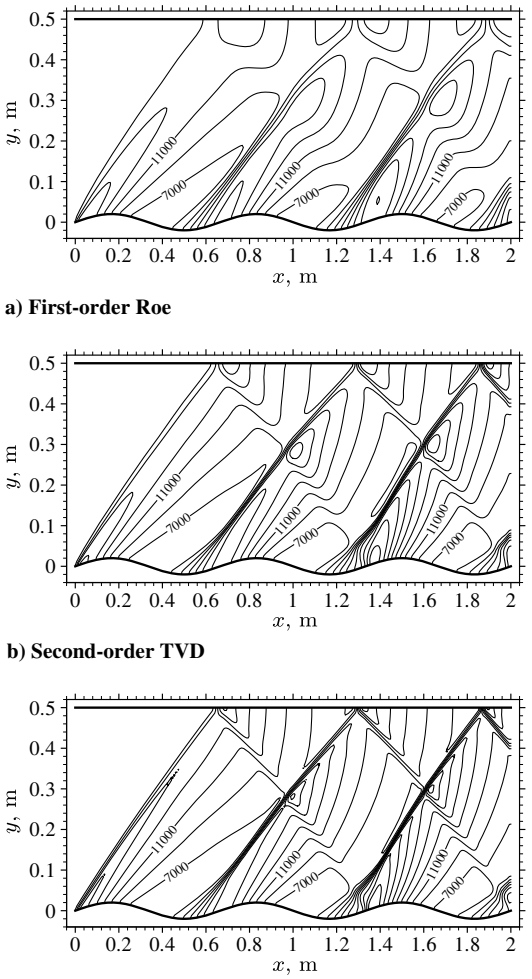

a) First-order Roe

b) Second-order TVD

c) Proposed first-order scheme

Fig. 2 Pressure contours in Pascals for the sine wall case using a 301×76 mesh.

wall located on the bottom of the channel, compression fans and expansion fans are generated (see Fig. 2). The compression fans converge into shock waves that reflect off the top of the channel and then interact with other waves emanating from the wavy wall. Because of the numerous wave interactions creating flow patterns that are difficult to capture well on coarse meshes, this serves as a capable test case to assess the capabilities of the numerical methods to solve inviscid Euler flow. From the pressure contours shown in Fig. 2, it is apparent that the proposed multidimensional scheme yields a higher resolution over its dimensionally split counterparts. The improvement in resolution can be seen to be uniform throughout the flowfield, being felt as much in the vicinity of the shock waves as within the compression and expansion fans.

In fact, despite the present method being first-order accurate, it exhibits a resolution as high as or higher than the one of a dimensionally split second-order-accurate TVD scheme (the Yee–Roe scheme [31]). This is confirmed in Table 1, where the average error on the density is tabulated for several meshes and where an estimate of the order of accuracy is given for various discretization schemes. It should not be surprising that the order of accuracy of the Yee–Roe TVD scheme only slightly exceeds one. As was shown by Goodman and Leveque in [34], the order of accuracy of dimensionally split TVD schemes is, at most, one when they are extended to multiple dimensions using dimensional splitting. It also should not be surprising that the proposed multidimensional method has an order of accuracy close to one: not only did we assume constant wave speeds in deriving the discretization equation from the Cauchy–Kowalevski procedure in Sec. II, but we made several changes to the discretization equation in Sec. IV to obtain monotonicity, which lead to the flux functions becoming first-order accurate. It is noted that the order of accuracy is here determined through the Richardson extrapolation, which is a technique that sometimes leads to dubious results for flows that include shock waves or other discontinuities, as in this case. However, it has been verified that the present method performs essentially the same and exhibits the same order of accuracy for some other flows that do not involve shocks/discontinuities, including the transonic Ringleb test case as well as a supersonic nozzle test case. In fact, for all cases considered, the present approach exhibited an order of accuracy slightly less than and never exceeding one, hence why it is here dubbed as first-order accurate. This is in contrast to the dimensionally split second-order-accurate TVD schemes that, albeit becoming first-order accurate for some two-dimensional (2-D) flows, do exhibit second-order accuracy for some other flows in which the waves more or less follow the grid lines (such as smoothly expanding nozzle flows).

It may be argued that, due to the various matrix multiplications involved within the cross-diffusion terms, the method proposed requires significantly more computing effort than the dimensionally split Roe scheme or even the Yee–Roe TVD scheme. However, as is shown in Table 2, the CPU time spent per iteration is about the same when the schemes are integrated using an implicit pseudotime stepping method (either block-implicit approximate factorization or diagonally dominant alternating-direction implicit [35]). This is due to the effort spent inverting the matrices when stepping in time implicitly being considerably greater than the effort spent on calculating the residual. Additional test cases indicate that the difference in CPU times between the various discretization strategies is further reduced for chemically reacting flows due to the considerable effort required to calculate the chemical reactions exceeding the effort spent calculating the residual of the convection derivatives.

Not only is the CPU time per iteration approximately the same between the proposed scheme and the dimensionally split TVD scheme, but so is the number of iterations necessary to reach convergence. Indeed, as shown in Table 3, there are minimal differences in the convergence rates exhibited by both schemes, either at low or high CFL numbers. Further, although the first-order Roe scheme is seen to converge more rapidly at a CFL number higher than eight, it can be argued that specifying such a high CFL number is not generally possible due to nonlinear stability restrictions. In fact, for many supersonic problems involving chemical reactions, strong shocks, or sharp fuel–air interfaces, the CFL number needs to be set to

Table 1 Percent error on the density and estimation of the order of accuracy using various schemes for the sine wall test case[a,b]

	$\frac{1}{(\rho S)_{\text{ref}}} \int_S \lvert\rho - \rho_{\text{exact}}\rvert \, \mathrm{d}S$		
Discretization scheme	101×26 nodes, %	401×101 nodes, %	Order of accuracy[c]
Dimensionally split first-order Roe	10.3	4.4	0.6
Dimensionally split second-order TVD	6.8	1.5	1.1
Proposed first-order method	6.2	1.9	0.9

[a]The exact solution is obtained using the Yee–Roe TVD scheme on a 3201×801 node mesh.

[b]The reference surface area S_{ref} is set to 1 m, and the reference density ρ_{ref} is set to 0.119 kg/m^3.

[c]The order of accuracy is estimated using Richardson extrapolation as $p = \ln(\epsilon_c/\epsilon_f)/\ln(\Delta x_c/\Delta x_f)$ with ϵ as the error and the subscripts c and f referring to the coarse and fine meshes, respectively.

Table 2 CPU time per iteration (in seconds) for the sine wall test case using a 301×76 mesh

Pseudotime stepping method	First-order Roe	Second-order TVD	Proposed method
Explicit Euler	0.100	0.121	0.173
Block-implicit approximate factorization	0.344	0.365	0.418
Diagonally dominant alternating-direction implicit [35]	0.447	0.469	0.522

Table 3 Number of iterations to reach convergence for the sine wall test case using a 301×76 mesh and block-implicit approximate-factorization pseudotime stepping[a]

CFL number	First-order Roe	Second-order TVD	Proposed method
1	1555	1526	1700
2	806	787	877
4	432	425	471
8	249	309	352
16	189	565	492

[a]Convergence is reached when the residual diminishes below a certain user-defined constant, which is fixed to the same value for all schemes and for all CFL numbers; this entails approximately seven orders of magnitude of convergence.

values not exceeding significantly one to prevent divergence to aphysical states. For such low CFL values, all schemes here considered are seen to display essentially the same convergence rates.

C. Supersonic Flow over a Blunt Body

Another test case that is commonly used to assess the capabilities of a numerical method in capturing shock waves is the simulation of supersonic airflow over a blunt body. The blunt body under consideration here consists of an ellipse with a width 2.4 times its height, whereas the incoming airflow is given a Mach number of three and zero angle of incidence. The mesh is composed of 33×33 nodes and is constructed such that the shock is aligned with the mesh on the axis of symmetry but becomes less and less aligned with the mesh as the distance from the axis of symmetry increases (see Fig. 3). The results are compared on the basis of the pressure coefficient that, for a thermally and calorically perfect gas, can be shown to be equal to

$$C_P = \frac{2(P - P_\infty)}{\gamma P_\infty M_\infty^2} \tag{42}$$

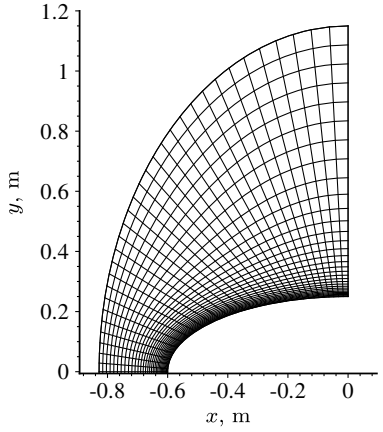

Fig. 3 Plot of the 33×33 mesh used for the Mach 3 blunt body test case.

As is generally recommended, the entropy correction is set to 0.3 for the acoustic waves in order to avoid a carbuncle. It is found necessary to further set the entropy correction to a small value of 0.02 for the nonacoustic waves to prevent aphysical phenomena from forming when using the proposed method. In Fig. 4, a comparison is performed between the proposed multidimensional scheme, a second-order TVD scheme, and the Huang–Lerat multidimensional method [26]. The pressure contour levels obtained with the Huang–Lerat method clearly show some oscillations in the vicinity of the shock when the mesh is not aligned with the shock wave, with the amount of pressure overshoot corresponding to about 15% of the pressure increase through the shock (see Fig. 4a). Such oscillations are nonexistent when using either the proposed multidimensional method or the second-order TVD scheme. In fact, the proposed first-order multidimensional scheme combines the best features of the Huang–Lerat method and the TVD scheme: similar to the Huang–Lerat method, it exhibits sharp expansion fans in the region between the body and the shock; and similar to the TVD scheme, it exhibits a monotone oscillation-free shock independent of the alignment of the mesh with respect to the shock wave.

It is noted, however, that the proposed method does exhibit somewhat lower resolution than the dimensionally split approach on the basis of pressure profiles on the axis of symmetry (see Fig. 5a), where the shock can be seen to be slightly more smeared. This is not a particular source of concern, however, because 1) this becomes less significant as the grid is refined (see Fig. 5b), and 2) this is limited to small regions and does not significantly affect the solution over the rest of the domain. Indeed, for many practical problems, the size of

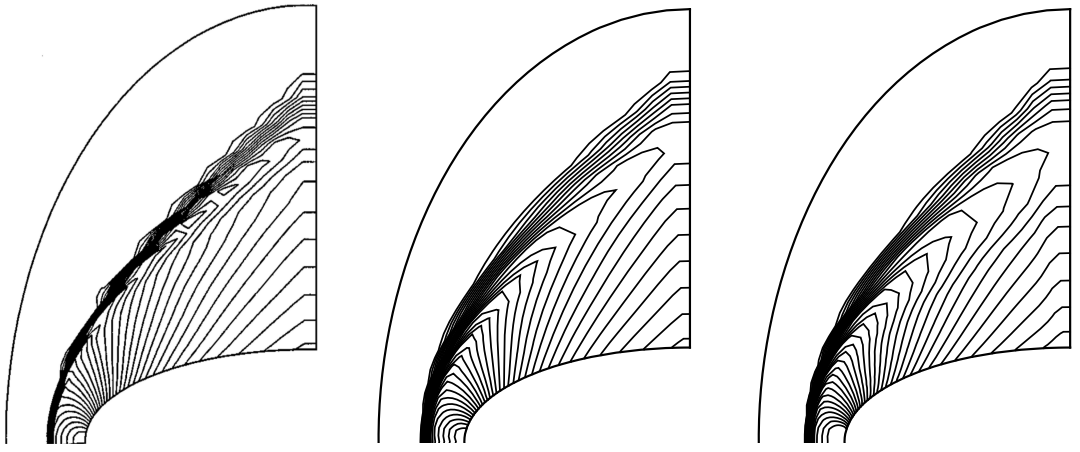

a) Huang-Lerat scheme [26] b) Proposed first-order scheme c) Second-order TVD scheme

Fig. 4 Pressure coefficient contours for the blunt body case with $\Delta C_P = 0.05$. Figure 4a is reprinted from [26] with permission from Elsevier.

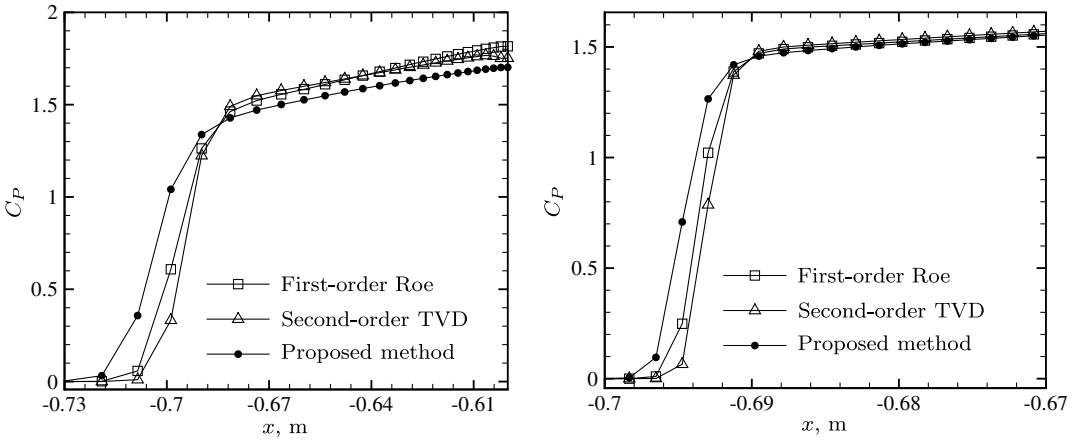

a) 33 × 33 mesh **b) 161 × 161 mesh**

Fig. 5 Pressure coefficient on the axis of symmetry for the blunt body case.

the regions where the shock is aligned with the grid is small due to difficulties in constructing a mesh that remains aligned with the shock in all locations.

D. Hypersonic Ramp Injector

Through the aforementioned test cases, it was demonstrated how the addition of cross-derivative terms to the Roe flux function can yield significant enhancements in resolution when solving expansion fans and shock waves, as well as shear waves. Another flow feature that necessitates investigation is the streamwise vortex occurring in some three-dimensional flowfields. One example of a streamwise vortex that is particularly difficult to simulate is the one generated by ramp injectors in scramjet inlets or combustors, with hydrogen or some hydrocarbon fuel being the injectant (see, for instance, [36] or [37]). To make the problem more easily reproducible, the injected fuel is here replaced by air with the inflow conditions being set as in Fig. 6. A surface of symmetry is imposed at $z \pm 28.6$ mm whereas the viscosity is fixed to 2×10^{-5} kg/ms and the thermal conductivity to 0.03 W/m K. Due to the incoming Mach number being in the hypersonic range, a strong bow shock forms above the injector. This leads to a large pressure difference between the top and side surfaces of the ramp, effectively inducing some streamwise vortices along the injector side surfaces. To minimize the impact of physical dissipation on the streamwise vortices, no turbulence model is added to the governing equations (the governing equations are hence limited to the mass conservation equation, the Navier–Stokes equations, and the total energy equation including thermal diffusion and viscous dissipation). Because of the low physical dissipation, the vortex retains its strength and continuously distorts and stretches the interface between the injected air and the incoming air throughout the mixing region. Such a flowfield is particularly difficult to capture due to the sharp interface between the injectant and the incoming flow moving rapidly in various directions and traveling obliquely to the grid lines, hence leading to a significant amount of numerical dissipation within the vortex. To assess the amount of dissipation introduced by the numerical method within the mixing region, a comparison between the steady-state temperature contours downstream of the point of injection is shown in Fig. 7 using a mesh comprising 8 million nodes. The temperature profiles show that the

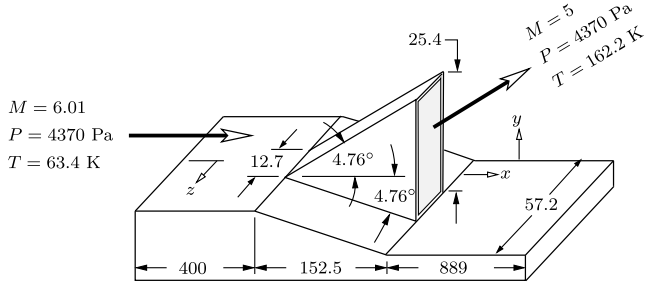

Fig. 6 Schematic of the ramp injector case with all dimensions in millimeters.

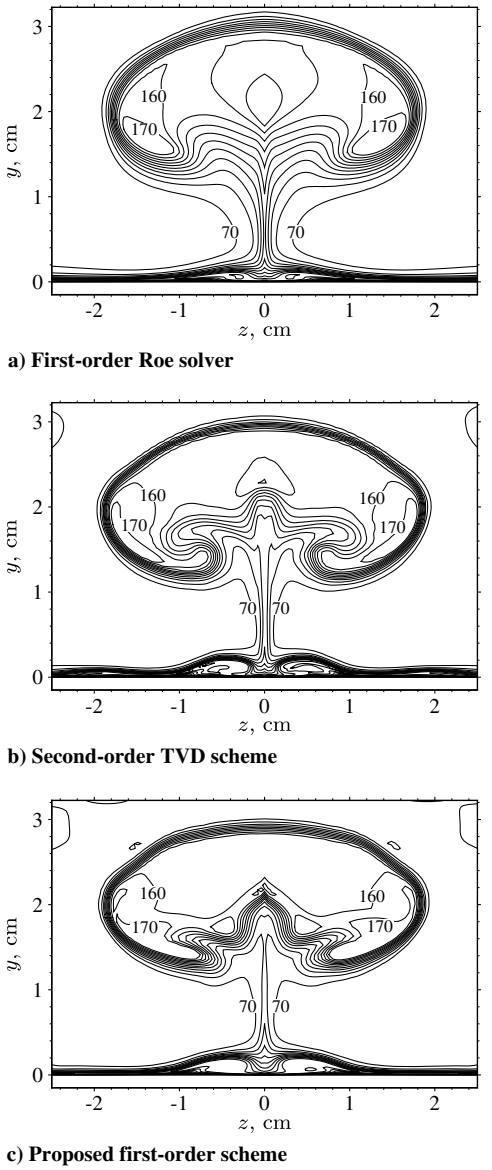

a) First-order Roe solver

b) Second-order TVD scheme

c) Proposed first-order scheme

Fig. 7 Temperature contours in Kelvin for the ramp injector case at $x = 0.02$ m using a 8-million-node mesh.

Table 4 Comparison between the proposed method and the dimensionally split first order approach on the basis of stagnation pressure difference for the ramp injector test case at $x = 0.2$ m[a]

		$\int_y\int_z \Delta P_s \, dz \, dy$, Pa · m^2	
Grid size	Number of nodes	First-order Roe	Proposed method
$205 \times 109 \times 85$	1,671,706	5687	5013
$406 \times 218 \times 167$	12,939,108	4904	4376
$811 \times 435 \times 333$	102,529,674	4479	4097

[a]The stagnation pressure difference ΔP_s corresponds to the difference between the freestream stagnation pressure and the local stagnation pressure determined from perfect gas relationships with the specific heat ratio set to 7/5.

proposed method reduces the amount of dissipation considerably compared to the first-order Roe scheme and even the second-order TVD scheme. As outlined in Table 4, a grid-convergence study shows that the proposed multidimensional method necessitates approximately 7–10 times fewer nodes to yield more or less the same solution as the dimensionally split first-order approach.

E. Subsonic Channel

The performance of the schemes is now assessed for a flow with negligible compressibility. Consider a low-speed inviscid subsonic flow in a 80-cm-long and 30-cm-high channel with a bump on the lower wall, as depicted in Fig. 8. The stagnation pressure and temperature are fixed at the inflow to 0.100702 bar and 300.6 K, and the pressure is fixed at the outflow boundary to 0.1 bar, whereas the other properties on the boundary nodes are extrapolated from the nearby inner nodes. This results in the flow Mach number remaining below 0.15 throughout the domain. Because the velocities are well below sonic, the density varies by less than 1% within the flowfield and the flow displays little compressibility. No entropy correction is hence needed for this case, although its use is found not to affect considerably the results. A comparison between the Mach number contours obtained using several meshes indicates that a substantial increase in resolution is achieved when using the proposed multidimensional scheme instead of the dimensional-splitting approach (see Fig. 8). This corresponds to more or less the same gains in accuracy as observed previously when solving highly compressible flows studded with compression fans, expansion fans, and shock waves. However, such gains in resolution become less pronounced when assessing pressure distribution on the surfaces as well as drag (which is here expected to be zero from theoretical considerations due to the flow being subsonic and inviscid in all locations). Although the proposed method fares better than the dimensionally split Roe scheme, it falls short of the dimensionally split second-order TVD scheme in predicting drag, as attested by the results shown in Table 5. This should not be particularly surprising, as we would expect the proposed method (which collapses to the first-order Roe scheme when the waves are aligned with the grid lines) not to yield as good a resolution as the dimensionally split second-order TVD scheme whenever the waves of importance are aligned with the mesh. Because the waves of importance when assessing drag for this problem are the pressure waves near the front and the back of the bump, and because the latter are somewhat aligned with the grid lines in such locations, the dimensionally split TVD scheme yields a better prediction of the overall drag force in this case compared to the proposed method.

Table 5 Comparison between the proposed method and the dimensionally split schemes on the basis of drag force for the subsonic channel test case

	Drag force, N	
Scheme	61^2 nodes	183^2 nodes
First-order Roe	2.07	0.96
Second-order TVD	0.78	−0.23
Proposed first-order method	1.94	0.83

F. Supersonic Boundary Layer

One appealing attribute of a numerical method that is often understated is the capability to resolve boundary layers with high resolution. Many flux discretization schemes (such as the Steger–Warming flux vector splitting method, the Harten–Lax–van Leer approximate Riemann solver, or the Jameson second–fourth order artificial dissipation schemes) introduce excessive dissipation in the boundary layer, making it difficult to obtain a grid-converged solution for practical problems that require an accurate prediction of the skin friction or boundary-layer thickness. On the other hand, the Roe scheme performs exceptionally well in this regard by introducing a minimal amount of dissipation within viscous layers. For instance, consider a laminar supersonic flow over a flat plate with the incoming air having a Mach number of two, a pressure of 0.1 bar, and a temperature of 300 K. Even when using a coarse mesh made of only

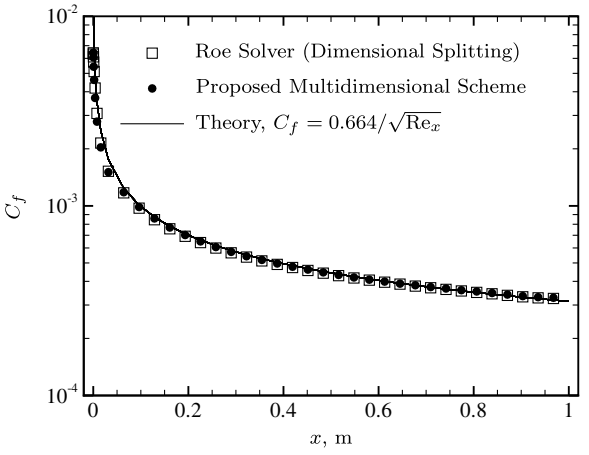

Fig. 9 Skin friction coefficient for the flat plate case.

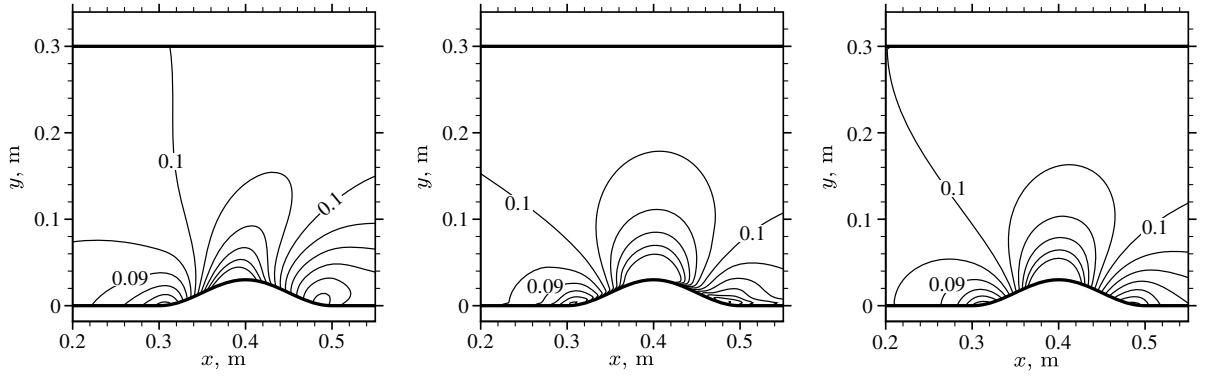

a) First-order Roe solver **b) Second-order TVD scheme** **c) Proposed first-order scheme**

Fig. 8 Mach number contours for the subsonic case with $\Delta M = 0.05$ using a 183×183 mesh.

40×50 nodes (with 60% of the gridlines distributed within 2 mm of the wall), the Roe scheme yields a skin-friction coefficient that is in very close agreement with the theoretical prediction. The small differences between the numerical results and the theoretical prediction are mostly due to the latter not being an exact solution to this problem, since it assumes no pressure gradient perpendicular to the plate. The proposed multidimensional method also exhibits exceptional accuracy for this problem, yielding a skin friction almost identical to the one of the dimensionally split approach throughout the length of the plate (see Fig. 9). Further, although not shown here for brevity, a comparison between the velocity contours as well as between the pressure contours reveals essentially no difference in solution between both approaches. That is, the proposed method yields a boundary-layer solution that is as monotonic and as free of dissipation as the one obtained with the conventional dimensionally split Roe solver.

VII. Conclusions

A novel genuinely multidimensional extension of the Roe flux difference splitting scheme is here proposed. The multidimensional terms are obtained along the lines of the Cauchy–Kowalevski procedure but differ from previous Cauchy–Kowalevski-based methods by yielding a solution that is essentially monotonic when solving strong oblique shocks or other discontinuities. The essentially monotonic property of the present scheme is obtained through a novel splitting of the cross-derivative terms along the different dimensions such that the cross-derivative coefficient remains small compared to the second-derivative coefficient. Although the method proposed does not satisfy the Harten condition, and is hence not monotonicity preserving per se, it does yield a solution that is essentially free of spurious oscillations.

Through several test cases involving both inviscid and viscous phenomena, it is demonstrated that the present approach generally achieves a significant twofold gain or more in resolution along each dimension when compared to the dimensional-splitting strategy. Gains in resolution have been observed for various types of flows ranging from quasi-incompressible subsonic to highly compressible hypersonic, not only within continuous waves (such as compression and expansion fans) but also in the vicinity of discontinuous waves (such as contact discontinuities and shocks). In fact, despite the flux discretization scheme presented herein being first-order accurate, numerical experiments indicate that it does yield a resolution as high as or higher than the one of dimensionally split second-order TVD methods for many flowfields.

What makes the aforementioned gains in resolution particularly noteworthy is that they are obtained while maintaining the appealing attributes of the first-order dimensionally split Roe solver. Indeed, similar to the latter, the proposed stencil has a compact three-node bandwidth (that is, the maximum width of the stencil is of three nodes along any dimension) and can be readily deployed to arbitrary systems of conservation laws because it is written in general matrix form (that is, the flux function depends only on the eigenvectors and eigenvalues of the convective flux Jacobian, which can be readily determined for any system of conservation laws). Further, the present approach is observed to capture boundary layers with high resolution and to converge as reliably as the dimensionally split Roe solver.

Another desirable attribute of the proposed scheme is its finite volume form. Specifically, the method is written as a flux function at the interface of cells, with the flux function not being a function of the time step or other relaxation parameters. As such, it can be used in conjunction with the multitude of acceleration techniques devised for finite volume schemes, such as multigrid, block-implicit approximate factorization, LUSGS, local pseudotime stepping, etc. In this paper, the various inviscid and viscous flowfields were obtained through a block-implicit approximate-factorization algorithm with local pseudotime stepping using CFL numbers ranging between 0.3 and 20. The addition of the multidimensional cross-difference terms are observed to result in small differences in the computing effort per iteration as well as in the number of iterations necessary to reach steady state.

Although the method presented herein is limited to first-order accuracy, it provides a framework that can be used to subsequently craft higher-order schemes that are both genuinely multidimensional and essentially monotonic. These are expected to considerably surpass in resolution the dimensionally split TVD schemes that are commonly used to solve compressible flows studded with strong shocks. The extension of the method to higher-order accuracy while keeping the solution essentially monotonic does present some challenges, however, and it is not clear at this stage how this can be achieved while maintaining the desirable attributes of the first-order scheme.

Appendix: Extension to Three Dimensions

Consider a system of conservation laws in differential form in three dimensions as follows:

$$\frac{\partial \boldsymbol{U}}{\partial t} + \frac{\partial \boldsymbol{F}}{\partial x} + \frac{\partial \boldsymbol{G}}{\partial y} + \frac{\partial \boldsymbol{H}}{\partial z} = 0 \tag{A1}$$

where $\boldsymbol{U}$ is the vector of conserved variables, whereas $\boldsymbol{F}$, $\boldsymbol{G}$, and $\boldsymbol{H}$ are the convective flux vectors along x, y, and z, respectively. When written in finite volume form, the discretization equation associated with the latter can be written as

$$\frac{\boldsymbol{U}^{n+1} - \boldsymbol{U}^{n}}{\Delta t} + \frac{\boldsymbol{F}_{i+1/2} - \boldsymbol{F}_{i-1/2}}{\Delta x} + \frac{\boldsymbol{G}_{j+1/2} - \boldsymbol{G}_{j-1/2}}{\Delta y} + \frac{\boldsymbol{H}_{k+1/2} - \boldsymbol{H}_{k-1/2}}{\Delta z} = 0 \tag{A2}$$

where $\boldsymbol{F}_{i+1/2}$, $\boldsymbol{G}_{j+1/2}$, and $\boldsymbol{H}_{k+1/2}$ denote the flux functions at the interfaces perpendicular to the x, y, and z axes, respectively. Then, following the same steps as in Secs. II–V, it can be shown that the proposed flux functions at the interfaces correspond to

$$\begin{aligned}\boldsymbol{F}_{i+1/2} = {} & \frac{1}{2}(\boldsymbol{F}_i + \boldsymbol{F}_{i+1}) \\ & - \frac{1}{2}|A|_{i+1/2}(\boldsymbol{U}_{i+1} - \boldsymbol{U}_i) \\ & - \frac{1}{4}B_{i+1/2}\left(\frac{\Delta y}{\Delta x}|A|_{i+1/2} + |B|_{i+1/2}\right)^{-1} A_{i+1/2}(\boldsymbol{U}_{i+1,j+1} \\ & - \boldsymbol{U}_{i+1,j-1} + \boldsymbol{U}_{i,j+1} - \boldsymbol{U}_{i,j-1}) \\ & - \frac{1}{4}C_{i+1/2}\left(\frac{\Delta z}{\Delta x}|A|_{i+1/2} + |C|_{i+1/2}\right)^{-1} A_{i+1/2}(\boldsymbol{U}_{i+1,k+1} \\ & - \boldsymbol{U}_{i+1,k-1} + \boldsymbol{U}_{i,k+1} - \boldsymbol{U}_{i,k-1})\end{aligned} \tag{A3}$$

$$\begin{aligned}\boldsymbol{G}_{j+1/2} = {} & \frac{1}{2}(\boldsymbol{G}_j + \boldsymbol{G}_{j+1}) \\ & - \frac{1}{2}|B|_{j+1/2}(\boldsymbol{U}_{j+1} - \boldsymbol{U}_j) \\ & - \frac{1}{4}A_{j+1/2}\left(\frac{\Delta x}{\Delta y}|B|_{j+1/2} + |A|_{j+1/2}\right)^{-1} B_{j+1/2}(\boldsymbol{U}_{i+1,j+1} \\ & - \boldsymbol{U}_{i-1,j+1} + \boldsymbol{U}_{i+1,j} - \boldsymbol{U}_{i-1,j}) \\ & - \frac{1}{4}C_{j+1/2}\left(\frac{\Delta z}{\Delta y}|B|_{j+1/2} + |C|_{j+1/2}\right)^{-1} B_{j+1/2}(\boldsymbol{U}_{j+1,k+1} \\ & - \boldsymbol{U}_{j+1,k-1} + \boldsymbol{U}_{j,k+1} - \boldsymbol{U}_{j,k-1})\end{aligned} \tag{A4}$$

$$\boldsymbol{H}_{k+1/2} = \frac{1}{2}(\boldsymbol{H}_k + \boldsymbol{H}_{k+1}) - \frac{1}{2}|C|_{k+1/2}(\boldsymbol{U}_{k+1} - \boldsymbol{U}_k) - \frac{1}{4}A_{k+1/2}\left(\frac{\Delta x}{\Delta z}|C|_{k+1/2} + |A|_{k+1/2}\right)^{-1} C_{k+1/2}(\boldsymbol{U}_{i+1,k+1} - \boldsymbol{U}_{i-1,k+1} + \boldsymbol{U}_{i+1,k} - \boldsymbol{U}_{i-1,k}) - \frac{1}{4}B_{k+1/2}\left(\frac{\Delta y}{\Delta z}|C|_{k+1/2} + |B|_{k+1/2}\right)^{-1} C_{k+1/2}(\boldsymbol{U}_{j+1,k+1} - \boldsymbol{U}_{j-1,k+1} + \boldsymbol{U}_{j+1,k} - \boldsymbol{U}_{j-1,k}) \quad \text{(A5)}$$

In the latter, A, B, and C correspond to the flux Jacobians, whereas $|A|$, $|B|$, and $|C|$ correspond to the Roe matrices along x, y, and z, respectively.

Acknowledgment

This work was supported for two years by a Pusan National University research grant.

References

[1] Raithby, G. D., "A Critical Evaluation of Upstream Differencing Applied to Problems Involving Fluid Flow," *Computer Methods in Applied Mechanics and Engineering*, Vol. 9, No. 1, 1976, pp. 75–103. doi:10.1016/0045-7825(76)90078-5

[2] Levy, D., Powell, K. G., and Van Leer, B., "Use of a Rotated Riemann Solver for the Two-Dimensional Euler Equations," *Journal of Computational Physics*, Vol. 106, No. 2, 1993, pp. 201–214. doi:10.1016/S0021-9991(83)71103-4

[3] Ren, Y.-X., "A Robust Shock-Capturing Scheme Based on Rotated Riemann Solvers," *Computers and Fluids*, Vol. 32, No. 10, 2003, pp. 1379–1403. doi:10.1016/S0045-7930(02)00114-7

[4] Nishikawa, H., "Very Simple, Carbuncle-Free, Boundary-Layer-Resolving, Rotated-Hybrid Riemann Solvers," *Journal of Computational Physics*, Vol. 227, No. 4, 2008, pp. 2560–2581. doi:10.1016/j.jcp.2007.11.003

[5] Roe, P. L., "Discrete Models for the Numerical Analysis of Time-Dependent Multidimensional Gas-Dynamics," *Journal of Computational Physics*, Vol. 63, No. 2, 1986, pp. 458–476. doi:10.1016/0021-9991(86)90204-4

[6] Deconinck, H., Roe, P. L., and Struijs, R., "A Multidimensional Generalization of Roe's Flux Difference Splitter for the Euler Equations," *Computers and Fluids*, Vol. 22, Nos. 2–3, 1993, pp. 215–222. doi:10.1016/0045-7930(93)90053-C

[7] Abgrall, R., and Mezine, M., "Construction of Second Order Accurate Monotone and Stable Residual Distribution Schemes for Unsteady Flow Problems," *Journal of Computational Physics*, Vol. 188, No. 1, 2003, pp. 16–55. doi:10.1016/S0021-9991(03)00084-6

[8] Abgrall, R., "Essentially Non-Oscillatory Residual Distribution Schemes for Hyperbolic Problems," *Journal of Computational Physics*, Vol. 214, No. 2, 2006, pp. 773–808. doi:10.1016/j.jcp.2005.10.034

[9] Abgrall, R., "Toward the Ultimate Conservative Scheme: Following the Quest," *Journal of Computational Physics*, Vol. 167, No. 2, 2001, pp. 277–315. doi:10.1006/jcph.2000.6672

[10] Roe, P. L., "Computational Fluid Dynamics—Restrospective and Prospective," *International Journal of Computational Fluid Dynamics*, Vol. 19, No. 8, 2005, pp. 581–594. doi:10.1080/10618560600585315

[11] van der Wiede, E., "Compressible Flow Simulations on Unstructured Grids Using Multi-Dimensional Upwind Schemes," Ph.D. Thesis, Delft Univ. of Technology, Delft, The Netherlands, 1998.

[12] Villedieu, N., Quintino, T., Ricchiuto, M., and Deconinck, H., "Third Order Residual Distribution Schemes for the Navier–Stokes Equations," *Journal of Computational Physics*, Vol. 230, No. 11, 2011, pp. 4301–4315. doi:10.1016/j.jcp.2010.12.026

[13] Nishikawa, H., "A First-Order System Approach for Diffusion Equation. I: Second-Order Residual-Distribution Schemes," *Journal of Computational Physics*, Vol. 227, No. 1, 2007, pp. 315–352. doi:10.1016/j.jcp.2007.07.029

[14] Nishikawa, H., "A First-Order System Approach for Diffusion Equation. II: Unification of Advection and Diffusion," *Journal of Computational Physics*, Vol. 229, No. 11, 2010, pp. 3989–4016. doi:10.1016/j.jcp.2009.10.040

[15] Nishikawa, H., "Robust and Accurate Viscous Discretization Via Upwind Scheme—I: Basic Principle," *Computers and Fluids*, Vol. 49, No. 1, 2011, pp. 62–86. doi:10.1016/j.compfluid.2011.04.014

[16] Lax, P. D., and Wendroff, B., "Difference Schemes for Hyperbolic Equations with High Order of Accuracy," *Communications on Pure and Applied Mathematics*, Vol. 17, 1964, pp. 381–398. doi:10.1002/(ISSN)1097-0312

[17] Richtmyer, R. D., "A Survey of Difference Methods for Non-Steady Gas Dynamics," National Center for Atmospheric Research TR-63-2, Boulder, CO, 1962.

[18] Smolarkiewicz, P. K., "A Fully Multidimensional Positive Definite Advection Transport Algorithm with Small Implicit Diffusion," *Journal of Computational Physics*, Vol. 54, No. 2, 1984, pp. 325–362. doi:10.1016/0021-9991(84)90121-9

[19] Colella, P., "Multidimensional Upwind Methods for Hyperbolic Conservation Laws," *Journal of Computational Physics*, Vol. 87, No. 1, 1990, pp. 171–200. doi:10.1016/0021-9991(90)90233-Q

[20] Leveque, R. J., "High-Resolution Conservative Algorithms for Advection in Incompressible Flow," *SIAM Journal on Numerical Analysis*, Vol. 33, No. 2, 1996, pp. 627–665. doi:10.1137/0733033

[21] Smolarkiewicz, P. K., and Margolin, L. G., "MPDATA: A Finite-Difference Solver for Geophysical Flows," *Journal of Computational Physics*, Vol. 140, No. 2, 1998, pp. 459–480. doi:10.1006/jcph.1998.5901

[22] Smolarkiewicz, P. K., "Multidimensional Positive Definite Advection Transport Algorithm," *International Journal for Numerical Methods in Fluids*, Vol. 50, No. 10, 2006, pp. 1123–1144. doi:10.1002/fld.1071

[23] Smolarkiewicz, P. K., and Szmelter, J., "Iterated Upwind Schemes for Gas Dynamics," *Journal of Computational Physics*, Vol. 228, No. 1, 2009, pp. 33–54. doi:10.1016/j.jcp.2008.08.008

[24] Ni, R.-H., "A Multiple-Grid Scheme for Solving the Euler Equations," *AIAA Journal*, Vol. 20, No. 11, 1982, pp. 1565–1571. doi:10.2514/3.51220

[25] Crumpton, P. I., Mackenzie, J. A., and Morton, K. W., "Cell Vertex Algorithms for the Compressible Navier–Stokes Equations," *Journal of Computational Physics*, Vol. 109, No. 1, 1993, pp. 1–15. doi:10.1006/jcph.1993.1194

[26] Huang, Y., and Lerat, A., "Second-Order Upwinding Through a Characteristic Time-Step Matrix for Compressible Flow Calculations," *Journal of Computational Physics*, Vol. 142, No. 2, 1998, pp. 445–472. doi:10.1006/jcph.1998.5935

[27] Toro, E. F., *Riemann Solvers and Numerical Methods for Fluid Dynamics*, 3rd ed., Springer, New York, 2009, p. 613.

[28] Smolarkiewicz, P. K., Khnlein, C., and Wedi, N. P., "A Consistent Framework for Discrete Integrations of Soundproof and Compressible PDEs of Atmospheric Dynamics," *Journal of Computational Physics*, Vol. 263, April 2014, pp. 185–205. doi:10.1016/j.jcp.2014.01.031

[29] Patankar, S. V., *Numerical Heat Transfer and Fluid Flow*, Taylor and Francis, Washington, D.C., 1980, p. 37.

[30] Roe, P. L., "Approximate Riemann Solvers, Parameter Vectors, and Difference Schemes," *Journal of Computational Physics*, Vol. 43, No. 2, 1981, pp. 357–372. doi:10.1016/0021-9991(81)90128-5

[31] Yee, H. C., Klopfer, G. H., and Montagné, J.-L., "High-Resolution Shock-Capturing Schemes for Inviscid and Viscous Hypersonic Flows," *Journal of Computational Physics*, Vol. 88, No. 1, 1990, pp. 31–61. doi:10.1016/0021-9991(90)90241-R

[32] Parent, B., "Positivity-Preserving High-Resolution Schemes for Systems of Conservation Laws," *Journal of Computational Physics*, Vol. 231, No. 1, 2012, pp. 173–189. doi:10.1016/j.jcp.2011.09.006

[33] Parent, B., and Sislian, J., "The Use of Domain Decomposition in Accelerating the Convergence of Quasi-Hyperbolic Systems," *Journal*

of Computational Physics, Vol. 179, No. 1, 2002, pp. 140–169.
doi:10.1006/jcph.2002.7048

[34] Goodman, J., and Leveque, R. J., "On the Accuracy of Stable Schemes for 2-D Scalar Conservation Laws," *Mathematics of Computation*, Vol. 45, No. 171, 1985, pp. 15–21.
doi:10.2307/2008046

[35] Bardina, J. E., "Three-Dimensional Navier–Stokes Method with Two-Equation Turbulence Models for Efficient Numerical Simulation of Hypersonic Flows," *30th Joint Propulsion Conference and Exhibit*, AIAA Paper 1994-2950, 1994.

[36] Parent, B., Sislian, J. P., and Schumacher, J., "Numerical Investigation of the Turbulent Mixing Performance of a Cantilevered Ramp Injector," *AIAA Journal*, Vol. 40, No. 8, 2002, pp. 1559–1566.
doi:10.2514/2.1824

[37] Parent, B., and Sislian, J. P., "Validation of the Wilcox kω Model for Flows Characteristic to Hypersonic Airbreathing Propulsion," *AIAA Journal*, Vol. 42, No. 2, 2004, pp. 261–270.
doi:10.2514/1.1989

W. K. Anderson
Associate Editor